Research Square

Preprints are preliminary reports that have not undergone peer review.
They should not be considered conclusive, used to inform clinical practice,
or referenced by the media as validated information.

# Frequency-Domain Attention-Guided Residual FCN] {Frequency-Domain Attention-Guided Residual Fully Convolutional Network for Seismic Thin-layer Resolution Enhancement

**Jiaxin Yang**
Yangtze University
**Yaming Yang**
Yangtze University
**Hua Zhang**
East China University of Technology
**Lang Yang**
China National Petroleum Corporation (China)
**Shuangjie Luo**
Key Laboratory of Engineering Geophysical Prospecting and Detection of Chinese Geophysical Society
**Wei Chen**
chenwei2014@yangtzeu.edu.cn

Yangtze University

**Research Article**

**Keywords:**

**Posted Date:** November 26th, 2026

**DOI:** https://doi.org/10.21203/rs.3.rs-9846085/v1

**License:** This work is licensed under a Creative Commons Attribution 4.0 International License.
Read Full License

**Additional Declarations:** No competing interests reported.

# Frequency-Domain Attention-Guided Residual Fully Convolutional Network for Seismic Thin-layer Resolution Enhancement

Jiaxin Yang[1], Yaming Yang[1], Hua Zhang[2], Lang Yang[3], Shuangjie Luo[4], Wei Chen[1,5*]

[1]Cooperative Innovation Center of Unconventional Oil and Gas (Ministry of Education & Hubei Province), Yangtze University, Wuhan, 430100, China.

[2]National Key Laboratory of Uranium Resources Exploration-Mining and Nuclear Remote Sensing, East China University of Technology, Nanchang, 330013, China.

[3]Tarim Branch Company of PetroChina, Korla, 841000, China.

[4]Sinopec Jianghan Oilfield Jianghan Oil Production Plant, Qianjiang, 433124, China.

[5]Key Laboratory of Engineering Geophysical Prospecting and Detection of Chinese Geophysical Society, Yangtze University, Wuhan, 430014, China.

*Corresponding author(s). E-mail(s): chenwei2014@yangtzeu.edu.cn;
Contributing authors: 3603817664@qq.com; yamingupc@126.com; hzhang@ecut.edu.cn; yangl2-tlm@petrochina.com.cn; 1364826984@qq.com;

**Abstract**

The band-limited nature of seismic data remains a fundamental bottleneck in the high-resolution characterization of thin-bed sequences. Driven by the intrinsic attenuation of subsurface media and the band-limited signature of the source wavelet, conventional spectral enhancement methods often struggle to balance bandwidth extension with signal-to-noise ratio (SNR) preservation. To address these challenges, we propose a seismic resolution enhancement framework based on a frequency-domain constrained residual fully convolutional network. Architecturally, the encoder incorporates a cascaded adaptive receptive field module,

utilizing parallel convolutional kernels ($\mathbf{7 \times 7}$, $\mathbf{5 \times 5}$, and $\mathbf{3 \times 3}$) to construct a multiscale feature hierarchy. This configuration facilitates the effective fusion of diverse seismic information, capturing a spectrum of geological signatures from macro-scale stratigraphic horizons to micro-scale thin-bed reflections. A novel frequency-domain residual block is introduced to implement explicit spectral attention via soft-thresholding, adaptively boosting effective frequency components while suppressing noise. In the decoding stage, $\mathbf{1 \times 1}$ convolutions and global residual connections are employed to facilitate the learning of sparse reflectivity residuals between low- and high-resolution data. The training process is supervised by a multi-domain joint loss function that integrates time-domain waveform matching, spectral alignment, and spatial structural consistency. Validations on both synthetic and field datasets demonstrate that the proposed method significantly broadens the effective bandwidth and delineates subtle thin-bed features. By achieving a substantial gain in vertical resolution while preserving lateral continuity, this research offers a robust high-fidelity solution for seismic signal processing.

**Keywords:** Seismic resolution, Deep learning, Multi-scale feature fusion, Frequency domain attention

# 1 Introduction

With the continuous advancement of global oil and gas exploration and development, exploration targets are increasingly shifting toward thin-layers, lithologic traps, and unconventional reservoirs characterized by complex geological conditions. These reservoirs typically exhibit small thicknesses and strong lateral heterogeneity, and their seismic responses often manifest as weak reflections, composite waves, or low signal-to-noise ratio (SNR) signals. Due to factors such as source excitation, subsurface absorption and attenuation, and constraints in acquisition and processing, conventional seismic data generally possess a narrow effective bandwidth. The energy is primarily concentrated in the low-to-medium frequency bands, with a severe deficiency in high-frequency components. Consequently, effectively broadening the bandwidth and enhancing the resolution of seismic data has remained a core research direction and a significant technical challenge in the field of seismic data processing.

To improve seismic resolution, geophysicists have developed various signal processing techniques. Common frequency-enhancement methods include deconvolution, spectral whitening, inverse Q-filtering, and weak signal enhancement. Deconvolution methods, based on seismic convolution theory, aim to compress the seismic wavelet into an approximate reflectivity series to improve resolution (Cao & Yang 2016; Chen et al. 2019). Furthermore, sparse spike inversion methods (Velis 2008), such as Basis Pursuit or Orthogonal Matching Pursuit (OMP), attempt to directly invert for the subsurface reflectivity coefficients, theoretically achieving the highest possible resolution. Oliveira & Lupinacci (2013) proposed an $L_1$-norm inversion method for estimating the reflectivity function in attenuating media, achieving efficient pulse compression and enhanced resolution. Building on this, Sui & Ma (2020) developed a blind sparse

spike deconvolution algorithm, which incorporates structural and sparsity constraints to simultaneously estimate the seismic wavelet and reflectivity coefficients, effectively improving the resolution of thin-layers.

Spectral whitening techniques enhance high-frequency energy by equalizing the amplitude spectrum without relying on the sparse reflectivity assumption inherent in deconvolution (Manenti et al. 2018). However, this approach often compromises the continuity of seismic reflection events, leading to the degradation of original waveform characteristics. To compensate for the high-frequency attenuation caused by formation absorption effects, researchers have employed inverse Q-filtering to recover both amplitude and frequency content (Wang 2002, 2006). Considering the non-stationary variations of wavelets in both time and space (Margrave et al. 2011), some studies have utilized the Gabor transform (Wang et al. 2013; Chen et al. 2013), the S-transform (Lin et al. 2022; Paksima et al. 2023), and Empirical Mode Decomposition (EMD) for frequency recovery. For instance, Chen et al. (2022) proposed a seismic time-frequency analysis method based on time-varying filtering, which adaptively calculates the cutoff frequency at each time step for mode decomposition. To further improve the suppression of random noise in non-stationary signals, Sun et al. (2020) developed an adaptive threshold denoising method based on Complementary Ensemble Empirical Mode Decomposition (CEEMD). Other bandwidth extension methods tailored for complex scenarios have also been developed, such as those targeting bandwidth enhancement for thin-layers (Wang et al. 2025), suppressing side lobes using Butterworth wavelets (Ji et al. 2022; Liu et al. 2026), and utilizing modified spectral bluing operators to enhance high-frequency information (Liu et al. 2023). While these traditional methods have proven effective, they often face limitations in balancing noise suppression with high-frequency recovery in highly complex geological settings.

In recent years, with the rapid advancement of computing power, deep learning (DL) technologies have achieved revolutionary breakthroughs in fields such as image processing and have rapidly permeated the geophysical domain (Oliveira et al. 2019; Harsuko & Alkhalifah 2022; Liu & Chen 2026). In the realm of seismic data pre-processing, DL has demonstrated superior performance in signal-to-noise ratio enhancement and data reconstruction. For example, Yang et al. (2023) utilized Convolutional Denoising Autoencoders (CDAE) to effectively suppress complex noise, while Yang et al. (2021) developed an adaptive convolutional neural network framework for seismic noise attenuation, which employs residual learning to improve training efficiency and incorporates batch normalization and leaky activation functions to enhance network performance in both synthetic and field data applications. Beyond pure denoising, Li et al. (2025) proposed an efficient unsupervised learning framework for simultaneous seismic noise attenuation and trace interpolation, ensuring data integrity for subsequent high-resolution processing.

These powerful nonlinear mapping capabilities provide a novel data-driven paradigm for addressing the challenges. For instance, Gao et al. (2023) and Chen et al. (2023) proposed seismic reflectivity inversion methods based on deep learning. By integrating the vertical reflectivity distribution of field data with lateral geological structural features, these methods can reconstruct high-resolution seismic data

through training. However, the generalization capability of networks remains a challenge when applied to datasets with different characteristics. To address this, Gao et al. (2022) incorporated structural constraints into a neural network framework to achieve high-resolution seismic reconstruction, while Deng et al. (2024) implemented seismic data reconstruction based on a conditional diffusion model, improving both prediction accuracy and generalization. Despite the immense potential shown by these DL methods in seismic resolution enhancement, several critical issues remain to be addressed. Most network models typically employ Mean Squared Error (MSE) or $L_1$ norm as loss functions. During the optimization process, these often lead to over-smoothed prediction results, thereby losing the high-frequency texture details crucial for thin-layer identification and causing deviations between the predicted spectrum and actual geological conditions (Li et al. 2021; Wang et al. 2024).

To mitigate this problem, Generative Adversarial Networks (GANs) have been introduced to seismic super-resolution reconstruction. Sun et al. (2022) utilized Super-Resolution GAN (SRGAN) to recover the high-frequency components of seismic data. However, the training instability of GANs and the potential for "hallucinated" textures pose significant challenges in seismic exploration (Wang et al. 2019). To capture multi-scale geological features, attention mechanisms have become research hotspots. Liu et al. (2023b) proposed an attention-based U-Net to improve inversion accuracy by weighting key regions. Das et al. (2019) designed a multi-scale residual network to enhance the characterization of complex structures. Recently, the Transformer architecture has also been introduced to seismic processing due to its global context modeling capabilities (Zhang et al. 2024). Since the essence of seismic resolution lies in the extension of the effective frequency band, simple time-domain losses often struggle to ensure phase consistency. In response, Alaei et al. (2018) reduced frequency distortion by introducing a spectral loss function, while Schuster et al. (2024) integrated Physics-Informed Neural Networks (PINNs) to ensure results comply with the wave equation. Building on these advances, Sun et al. (2021) further explored physics-guided deep learning for seismic inversion using hybrid training data. In light of the difficulties in thin-layer identification and the insufficient high-frequency recovery of conventional networks, this paper develops a seismic resolution enhancement method based on a frequency-domain constrained residual fully convolutional network. This method innovatively constructs a dual-path feature extraction mechanism to achieve resolution enhancement via end-to-end mapping. On one hand, the dual-path design captures both deep semantic features and shallow high-frequency details. On the other hand, by introducing a frequency-domain constraint as a regularization term, the network is forced to correct the spectral morphology while recovering time-domain waveforms. Through application to both synthetic and field data, the proposed method demonstrates significant advantages in broadening the effective bandwidth while preserving structural integrity.

## 2 Methodology

The core challenge of deep learning-based resolution enhancement lies in acquiring a large volume of high-quality, paired samples consisting of low-resolution (LR) inputs

and high-resolution (HR) labels. While traditional forward modeling methods can generate noise-free data, they often fail to fully simulate the inherent complexity of real subsurface media, thereby limiting the model's generalization capability.

## 2.1 Exploration and Establishment of High-Quality Labels

The performance ceiling of a deep learning model is fundamentally determined by the quality of its training labels. In the field of seismic exploration, obtaining the true reflectivity or broadband seismic response across an entire survey area presents an inherent challenge. To avoid the assumption errors introduced by direct synthetic data from theoretical models, and to overcome the lateral discontinuities often associated with conventional trace-by-trace deconvolution, this paper proposes a label generation strategy characterized by physics-guided construction and well-log-driven calibration. The objective of this strategy is to construct an ideal seismic dataset that exhibits lateral continuity, accounts for vertical non-stationary attenuation, and maintains high fidelity to well-log responses at well locations, serving as the training target for the network.

The core concept involves designing a unified, time-invariant zero-phase enhancement filter for the entire section. Let $\bar{A}(f)$ represent the average amplitude spectrum of the entire seismic section $D(t, x)$, which is utilized to capture the global frequency characteristics of the profile:

$$\begin{aligned} \hat{D}(f, x) &= \mathcal{F}_t\{D(t, x)\}, \\ \bar{A}(f) &= \frac{1}{N_x} \sum_{x=1}^{N_x} |\hat{D}(f, x)| \end{aligned} \tag{1}$$

where $\mathcal{F}_t$ denotes the one-dimensional Fourier transform along the time axis, and $N_x$ represents the total number of seismic traces. A parameterized gain function, $G(f)$, is designed to reshape the amplitude spectrum. The objective of this function is to preserve low-frequency components, enhance medium-to-high frequencies, and suppress ultra-high-frequency noise. Its primary component is defined by a linear enhancement ramp:

$$G(f) = 1 + (G_{\max} - 1) \frac{f - f_{\text{start}}}{f_{\text{end}} - f_{\text{start}}}, \quad \text{for } f \in [f_{\text{start}}, f_{\text{end}}] \tag{2}$$

where $G_{\max}$ represents the maximum gain amplitude, while $f_{\text{start}}$ and $f_{\text{end}}$ denote the start and end frequencies of the enhancement band, respectively. By utilizing the gain function as the amplitude spectrum of a zero-phase filter, the enhancement is applied to the spectrum $\hat{D}(f, x)$ of the entire seismic section as follows:

$$\begin{aligned} \hat{D}_{\text{enhanced}}(f, x) &= \hat{D}(f, x) \cdot G(f), \\ D_{\text{enhanced}}(t, x) &= \mathcal{F}_t^{-1} \left\{ \widehat{D}_{\text{enhanced}}(f, x) \right\} \end{aligned} \tag{3}$$

As seismic waves propagate, they exhibit non-stationary characteristics where high-frequency energy undergoes exponential attenuation with depth. This phenomenon

often leads to the excessive amplification of background noise in deeper layers, thereby limiting the reliability of the processed data as a global label. To address this issue, a time-varying weight function, $W(t)$, is defined in this study to dynamically adjust the enhancement intensity:

$$W(t) = \frac{1}{1 + e^{-k(t-t_0)}} \tag{4}$$

where $t_0$ represents the center time of the transition zone, and $k$ controls the steepness of this transition. The final label section $L(t, x)$ is obtained through a weighted fusion of the previously enhanced result $D_{\text{enhanced}}(t, x)$ and the original data $D_{\text{orig}}(t, x)$:

$$L(t, x) = D_{\text{enhanced}}(t, x) \cdot W(t) + D_{\text{orig}}(t, x) \cdot (1 - W(t)) \tag{5}$$

The final labels generated through this workflow not only possess high resolution and clarity in the shallow sections but also maintain stability and fidelity in the deep layers. While the aforementioned physics-guided strategy is inherently reasonable, the setting of its parameters (such as $G_{\max}$, $f_{\text{start}}$, and $f_{\text{end}}$) remains somewhat subjective. To anchor the physical priors to real geological data, we introduce a well-controlled calibration mechanism. This mechanism adopts high-resolution synthetic seismograms from well logs within the survey area as the local geological ground truth. By minimizing the discrepancy between the enhanced seismic traces and the synthetic records, the originally subjective parameter settings are transformed into a data-driven constrained optimization problem.

Figure 1 displays a representative example of the generated training labels. Traditional methods (Fig. 1b) exhibit prominent vertical stripe artifacts and high-frequency random noise in the deep layers due to the lack of physical constraints. In contrast, the final labels after well-controlled calibration (Fig. 1c) show clear and continuous reflection characteristics. The residual profile shown in Fig. 1d further confirms the effectiveness of the calibration, providing an ideal supervision target for the deep learning network.

## 2.2 Network Architecture

To address the issue of spectral blindness inherent in traditional fully convolutional networks (FCNs) when processing seismic signals, this paper proposes a Frequency-Domain Constrained Residual Fully Convolutional Network (FGC-Net). While maintaining the advantages of the FCN architecture in handling sequences of arbitrary length, FGC-Net introduces a frequency-domain guidance mechanism. This represents a paradigm shift from purely data-driven to physics-guided learning, effectively resolving the challenges of amplitude preservation and artifact suppression in seismic signal enhancement.

As illustrated in Fig. 2, FGC-Net adopts an encoder-decoder architecture. Its core innovation lies in the construction of a dual-path feature extraction mechanism that achieves end-to-end mapping of raw waveforms to significantly enhance vertical resolution. The network takes a single-trace band-limited seismic record $X \in \mathbb{R}^{1\times L}$ as input, where $L$ denotes the length of the time series. The encoder aims to map seismic data from the time-domain space to a high-dimensional latent feature space. It

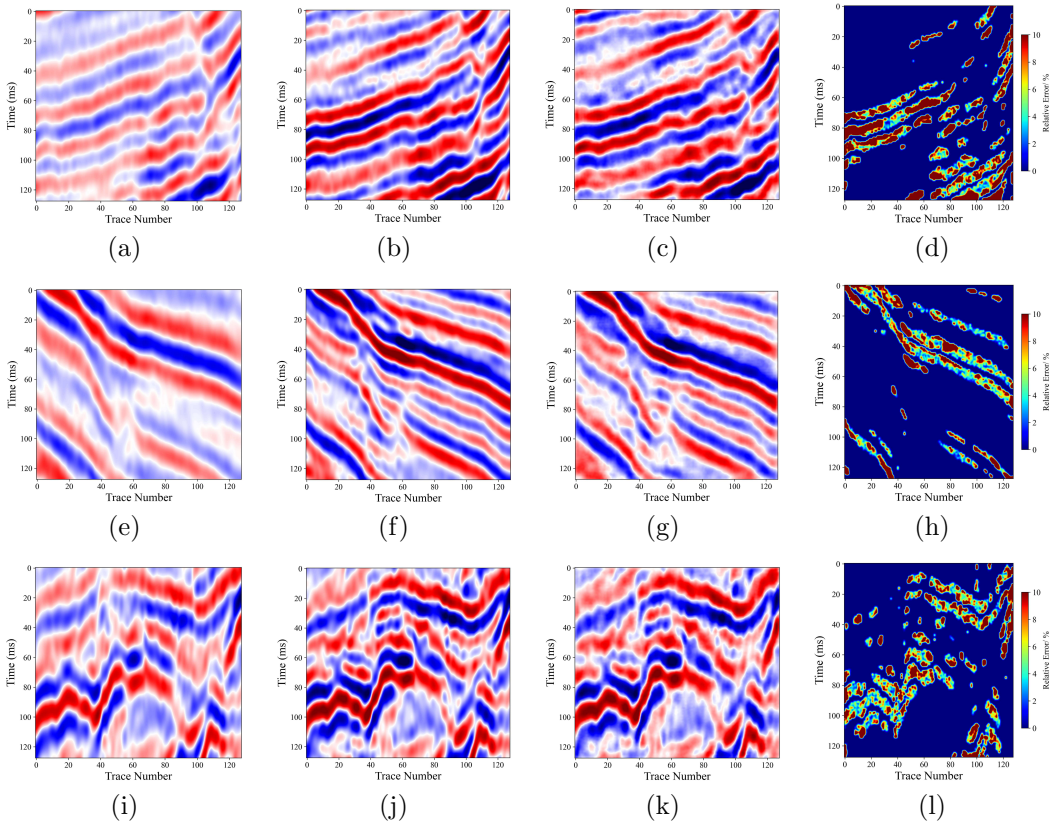


**Fig. 1** Training data examples across three different geological scenarios (Rows 1–3). **a**, **e**, **i** Original low-resolution seismic data; **b**, **f**, **j** results from the unconstrained network; **c**, **g**, **k** high-quality labeled data after well control correction; **d**, **h**, **l** corresponding relative error profiles

comprises three cascaded Receptive Field Adaptive Modules (RFAM). These modules utilize convolutional kernel sizes of 7, 5, and 3, respectively, to form a multi-scale feature pyramid. This design is intended to simultaneously capture multi-scale features ranging from macroscopic seismic events to microscopic thin-layer reflections.

To overcome the tendency of deep networks to lose high-frequency details, we append an innovative Frequency-Domain Residual Block (FRB) after each RFAM. By employing an explicit frequency-domain attention mechanism, this module performs soft-thresholding filtering on the feature maps, effectively isolating the effective signal bandwidth from noise components. In the decoder section, the network utilizes $1 \times 1$ convolutions for feature fusion and channel adjustment, ensuring the effective integration of multi-scale features. Finally, through a global residual connection at the end of the network, the learned residual signal is added to the original input to output the high-resolution seismic record $Y \in \mathbb{R}^{1\times L}$. This design compels the network to focus on learning the relative residual, which significantly reduces the training difficulty while ensuring that the enhanced signal maintains amplitude consistency with the original input.

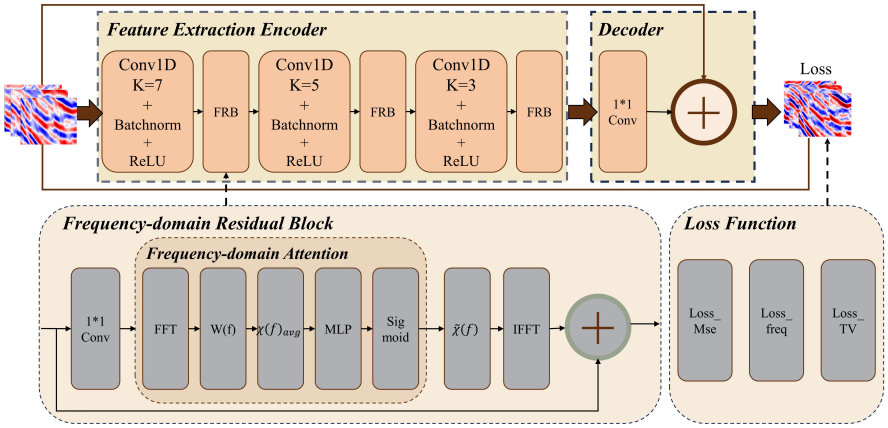


**Fig. 2** Architecture of the proposed Frequency-Domain Constrained Residual Fully Convolutional Network (FGC-Net). The encoder consists of cascaded Receptive Field Adaptive Modules (RFAMs) and Frequency-Domain Residual Blocks (FRBs). The decoder uses $1 \times 1$ convolutions and a global skip connection to output the high-resolution trace

Seismic signals are non-stationary, and geological structures exhibit vast differences across various depths and scales. Macroscopic structural contexts require a larger receptive field to capture low-frequency trends, whereas minute geological anomalies rely on localized, subtle features. Traditional fixed-size convolutional kernels struggle to balance these two requirements. Based on the principle of multi-scale perception, the RFAM acquires features ranging from macroscopic trends to microscopic details by cascading kernels of different sizes. The operation of an RFAM can be expressed as a combination of convolutions and non-linear activations. To construct the feature pyramid, we set specific convolutional kernel sizes $k_i \in \{7, 5, 3\}$ for the shallow, middle, and deep layers of the encoder. The output features $F^i_{\text{rfam}}$ of the $i$-th layer are calculated as:

$$F^i_{\text{rfam}} = \sigma\left(\text{BN}\left(\text{Conv}^{k_i}_{\text{1D}}\left(F^i_{\text{in}}\right)\right)\right) \tag{6}$$

where $F^i_{\text{in}}$ represents the input feature of the $i$-th encoder layer, $\text{Conv}^{k_i}_{\text{1D}}$ denotes a one-dimensional convolutional operation with a kernel size of $k_i$, BN is Batch Normalization, and $\sigma$ is the PReLU activation function. As the network depth increases, the convolutional kernel sizes gradually decrease following a 7-5-3 pyramid configuration. This setup enables the network to adaptively encode seismic records: larger kernels in the shallow layers act as low-pass filters to stabilize the global structural framework, while smaller kernels in the deeper layers function as high-pass filters to acutely capture high-frequency responses caused by abrupt changes in reflectivity. This provides a rich, multi-scale feature foundation for subsequent frequency-domain processing.

The Frequency-Domain Residual Block (FRB) is designed to embed frequency-domain prior knowledge into the underlying network layers to achieve dynamic bandwidth constraints. During the forward propagation process, this module transforms convolutional features into the frequency domain and utilizes a lightweight attention network to learn the importance weights of various frequency components.

This allows the network to autonomously identify and enhance frequency components associated with effective reflections. Specifically, for a given input feature map $X \in \mathbb{R}^{B\times C\times L}$, a one-dimensional Fast Fourier Transform (FFT) is first performed:

$$X(f) = \mathcal{F}(X) \tag{7}$$

Next, a frequency-domain channel attention mechanism is designed to learn the spectral weights $W(f)$. These weights are generated through a sub-network consisting of two fully connected (FC) layers and a Sigmoid activation function, thereby capturing the dependencies between frequency channels:

$$M(f) = \sigma\left(W_2\delta\left(W_1 X(f)_{\text{avg}}\right)\right) \tag{8}$$

where $M(f)$ is the learned spectral mask, and $X(f)_{\text{avg}}$ represents the global average pooling of the spectral magnitude. Subsequently, the mask is applied to the original spectrum:

$$\widetilde{X}(f) = X(f) \odot M(f) \tag{9}$$

Finally, the result is transformed back to the time domain via the Inverse Fast Fourier Transform (IFFT), and a residual connection is introduced to accelerate gradient backpropagation:

$$Y = \mathcal{F}^{-1}(\widetilde{X}(f)) + X \tag{10}$$

The FRB serves as the core correction unit of FGC-Net. Positioned after each RFAM, it functions as a learnable band-pass filter. While the network attempts to recover high-frequency information, the FRB automatically suppresses anomalous spectral spikes, ensuring that the output seismic waveforms possess a reasonable energy distribution across the spectrum. Consequently, this guarantees the fidelity of the resolution enhancement at a physical level.

## 2.3 Loss Function

To compel FGC-Net to approximate high-resolution ground-truth records in terms of both waveform similarity and spectral structure, we designed a multi-domain joint loss function:

$$\mathcal{L}_{\text{total}} = \mathcal{L}_{\text{MSE}} + \alpha \cdot \mathcal{L}_{\text{freq}} + \beta \cdot \mathcal{L}_{\text{TV}} \tag{11}$$

where $\mathcal{L}_{\text{MSE}}$ is the Mean Squared Error loss, ensuring the accurate reconstruction of time-domain waveforms. $\mathcal{L}_{\text{freq}}$ represents the spectral discrepancy loss between the output and target signals, which directly constrains the frequency-band characteristics of the enhancement results to align with the high-resolution targets. $\mathcal{L}_{\text{TV}}$ is the Total Variation (TV) regularization term, utilized to maintain the lateral continuity of the output signals. It effectively preserves the spatial coherence of seismic events and prevents waveform fragmentation caused by over-enhancement. The hyperparameters $\alpha$ and $\beta$ are used to balance the relative importance of each loss component.

The frequency-domain matching loss is implemented by calculating the difference between the amplitude spectra of the output and the target signals:

$$\mathcal{L}_{\text{freq}} = \frac{1}{N} \sum_{i=1}^{N} \| |\mathcal{F}(y_i)| - |\mathcal{F}(\hat{y}_i)| \|_2^2 \tag{12}$$

where $y_i$ and $\hat{y}_i$ denote the target signal and the network output, respectively, and $N$ represents the batch size. The Total Variation regularization term enhances lateral continuity by penalizing discrepancies between adjacent sampling points:

$$\mathcal{L}_{\text{TV}} = \sum_{i,j} \left( |\hat{y}_{i+1,j} - \hat{y}_{i,j}| + |\hat{y}_{i,j+1} - \hat{y}_{i,j}| \right) \tag{13}$$

This multi-constraint optimization strategy ensures that the network maintains amplitude fidelity and geological plausibility while improving resolution. By embedding frequency-domain constraints into both the network architecture and the optimization objective, FGC-Net achieves guided enhancement of seismic signals, demonstrating significant advantages particularly in thin-layer identification and noise suppression.

# 3 Model Testing

To evaluate the performance of the proposed method in thin-layer identification and side-lobe suppression, a 2D acoustic velocity model was constructed. This model contains two thin-layers of specified thicknesses and a wedge body with varying thickness. Noise-free synthetic records were generated using a Ricker wavelet with a dominant frequency of 25 Hz, as shown in Fig. 3. The model consists of 50 traces with a vertical sampling interval of 0.5 m. The background velocity is set as a layered distribution increasing from 2000 m/s to 2750 m/s. Two horizontal thin-layers are designed at depths of 100 m and 200 m, with velocities of 2200 m/s and 2350 m/s, respectively, to test the method's ability to identify weak impedance contrasts between layers. At a depth of 300 m, a wedge body with a velocity of 2600 m/s is embedded within host rock of 2750 m/s. The wedge thickness decreases linearly from 50 m at Trace 0 to 0 m at Trace 50, providing a continuously varying thickness sequence to precisely determine the tuning thickness and resolution limit of different methods.

Fig. 4 visually demonstrates the analytical capability of different methods regarding complex interference wavefields. The dashed and solid lines mark the $\lambda/4$ tuning thickness and the $\lambda/8$ limit of resolution corresponding to the 25 Hz dominant frequency, respectively.

Fig. 4**a** shows the original record; due to tuning effects, the top and bottom reflection events merge when the wedge thickness is less than the $\lambda/4$ tuning thickness, making it impossible to distinguish the thin-layer boundaries. The horizontal thin-layer regions also appear as wide composite wavelets.

Comparing the results of Inverse Q-filtering (IQF) in Fig. 4**b** and the U-Net result in Fig. 4**c**, it can be observed that while traditional methods compress the wavelet to some extent, the waveforms still exhibit smearing in the extremely thin regions near

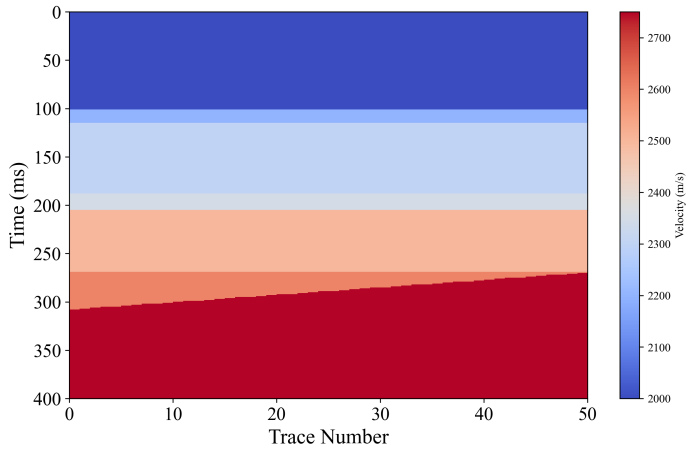


**Fig. 3** Noise-free synthetic velocity model

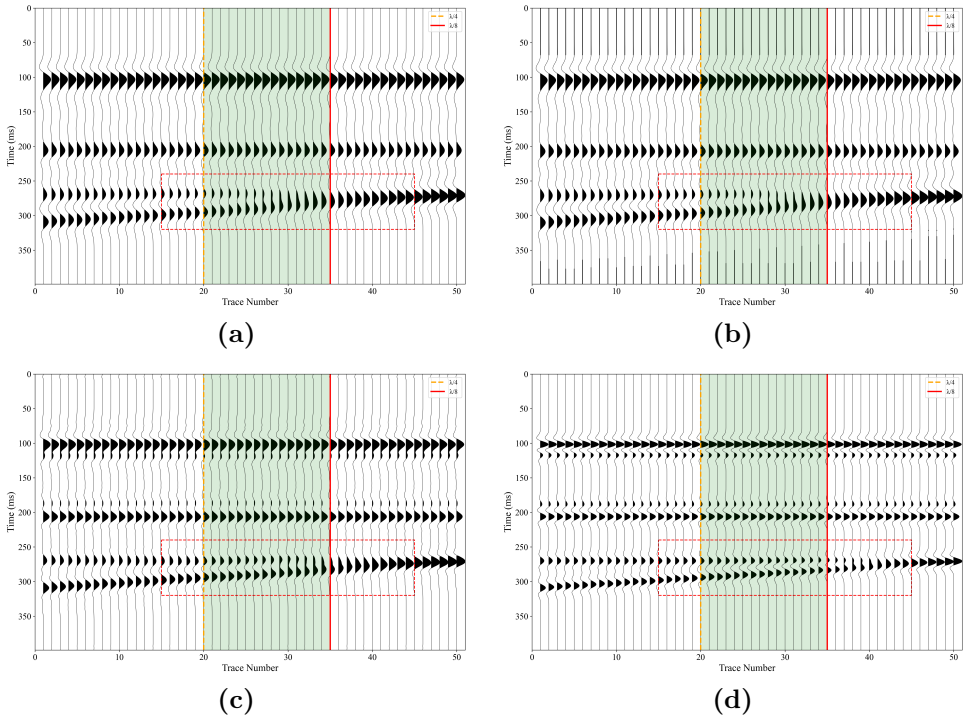


**Fig. 4** Processing results on the wedge model. **a** Original low-resolution record; **b** Inverse Q-filtering (IQF) result; **c** U-Net result; **d** Result of the proposed FGC-Net. Dashed and solid lines indicate $\lambda/4$ and $\lambda/8$ resolution limits

the $\lambda/8$ resolution limit. Furthermore, the IQF method introduces Gibbs phenomena, leading to enhanced side-lobe artifacts. While the conventional U-Net significantly

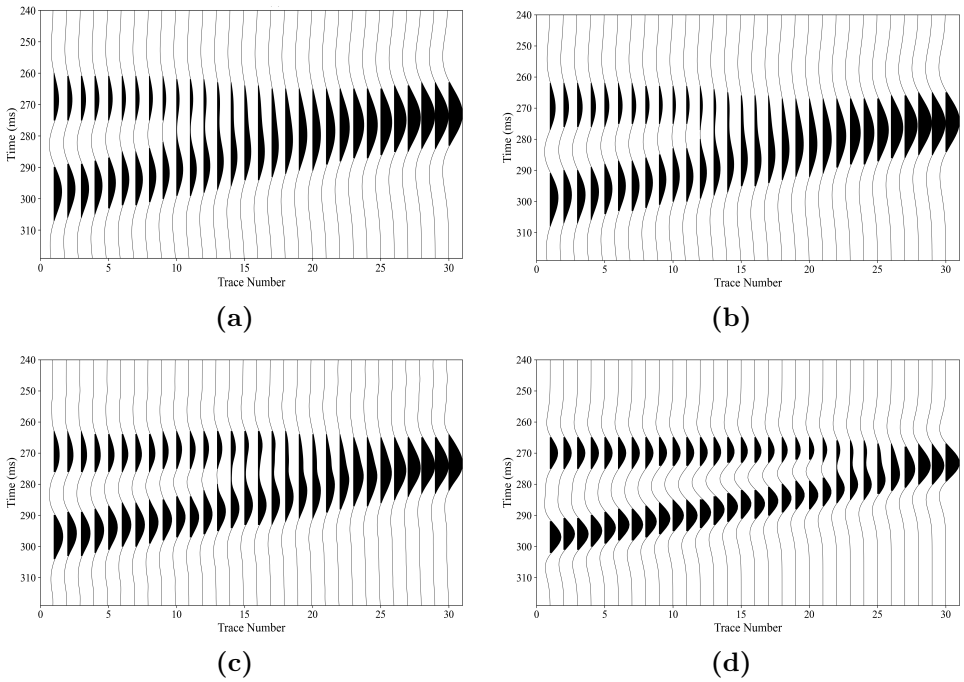


**Fig. 5** Magnified views of the red rectangular areas indicated in Figure 4. **a** Original synthetic record; **b** IQF result; **c** U-Net result; **d** Result of the proposed FGC-Net

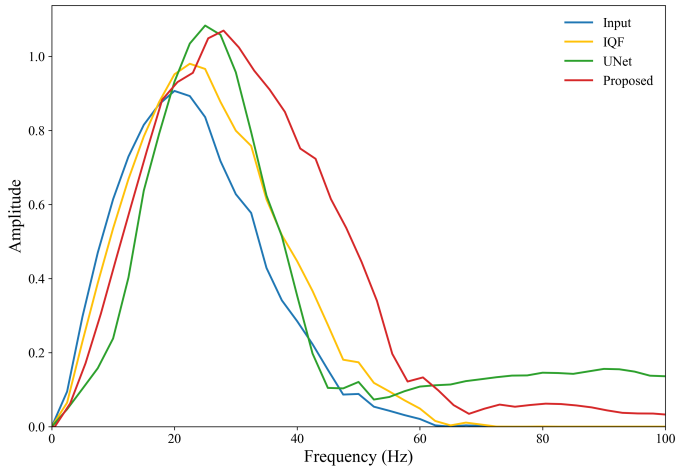


**Fig. 6** Comparison of Amplitude spectra

improves resolution compared to the original data and identifies most of the wedge boundaries, the waveform recovery between Traces 40–50 is not sharp enough, and the amplitude fidelity is slightly deficient.

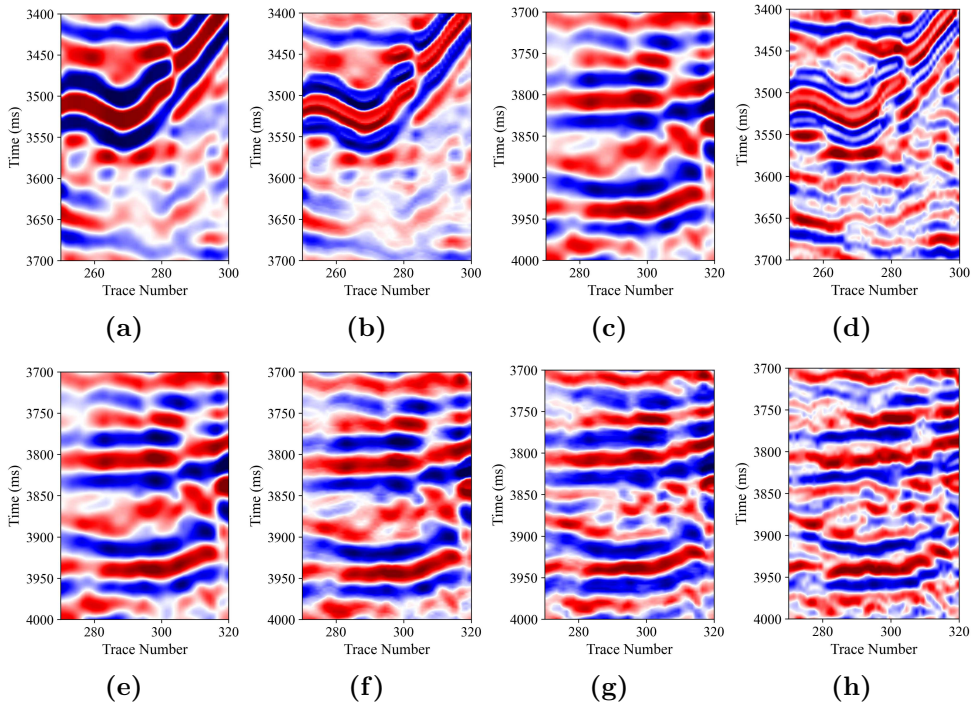


**Fig. 7** Magnified views of the low-resolution data and processing results. **a** and **e** Original low-resolution data; **b** and **f** IQF result; **c** and **g** U-Net result; **d** and **h** Results of the proposed method

In contrast, the proposed method (Fig. 4**d**) not only successfully separates the top and bottom reflections into two independent events at the $\lambda/4$ tuning thickness but also maintains clear waveform separation in extremely thin regions approaching the $\lambda/8$ resolution limit.

To further evaluate the local detailed texturing, Fig. 5 highlights the magnified views of the area within the red rectangular box where the wedge thickness decreases sharply. The original synthetic record (Fig. 5**a**), IQF result (Fig. 5**b**), and U-Net result (Fig. 5**c**) exhibit varying degrees of vertical smearing and resolution degradation in the ultra-thin pinch-out zone. By contrast, the interlayer interfaces of the two horizontal thin-layers are characterized more sharply with a clean background by the proposed method (Fig. 5**d**), proving that the network architecture effectively suppresses artifacts while enhancing the dominant frequency.

In addition to the qualitative spatial analysis, the comparison of average amplitude spectra in Fig. 6 provides a quantitative assessment of the resolution enhancement. The spectra indicate that the proposed method (red curve) increases the dominant frequency from 22 Hz to approximately 38 Hz, significantly broadening the effective bandwidth. Simultaneously, the method excellently preserves low-frequency energy, overcoming the drawback of traditional frequency enhancement methods that tend to damage low-frequency structural information.

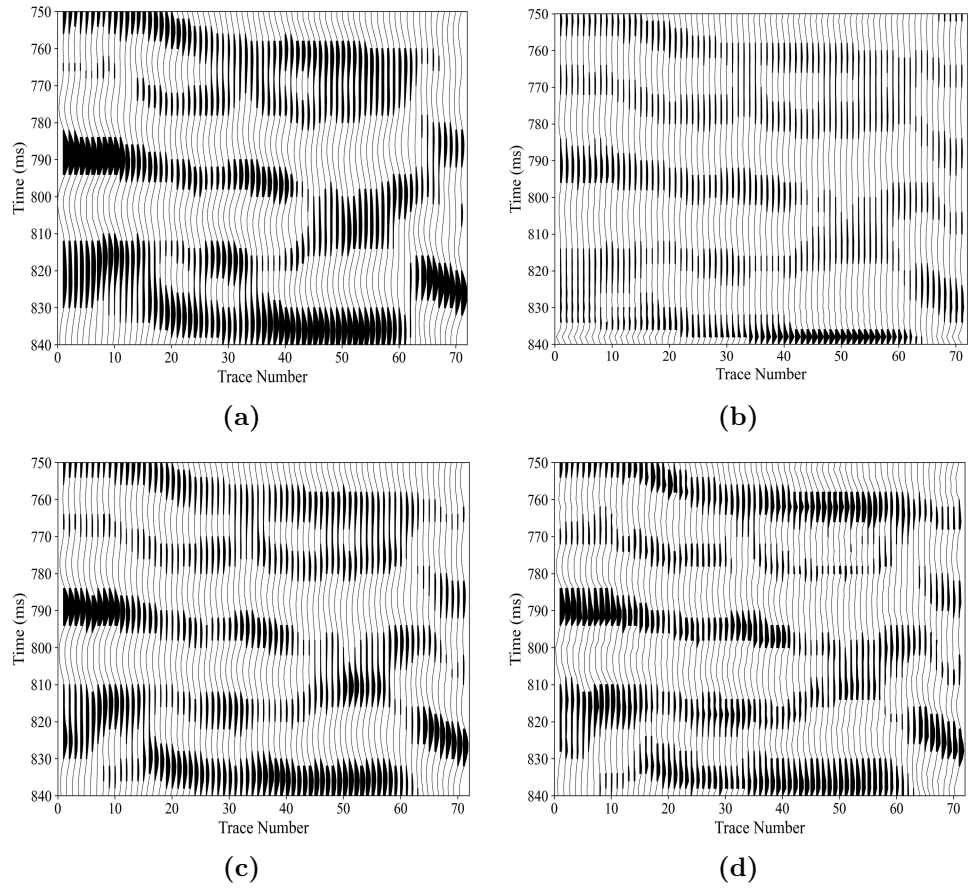


**Fig. 8** Magnified views of the low-resolution data and processing results. **a** Original low-resolution data; **b** IQF result; **c** U-Net result; **d** Result of the proposed method

# 4 Field Data Application

The target seismic field data are acquired from a typical layered sedimentary sequence characterized by complex thin-bed interbedding and subtle structural variations. Due to the severe attenuation of high-frequency components during wave propagation, the raw seismic reflections suffer from significant vertical interference, posing a major challenge for the identification of fine-scale geological features. Fig. 7 illustrates the processing results of different methods in a layered sedimentary region, where a local sub-section was selected for detailed analysis.

The original seismic section (Fig. 8**a**) exhibits a low dominant frequency, which causes adjacent thin-layer reflections to interfere with each other, forming broad, low-frequency seismic events. In this section, fault points and subtle fold features are blurred, making it impossible to perform fine-grained geological layering. Although the IQF method (Fig. 8**b**) compresses the wavelet to a certain extent, the overall resolution improvement is limited. While the conventional U-Net method (Fig. 8**c**)

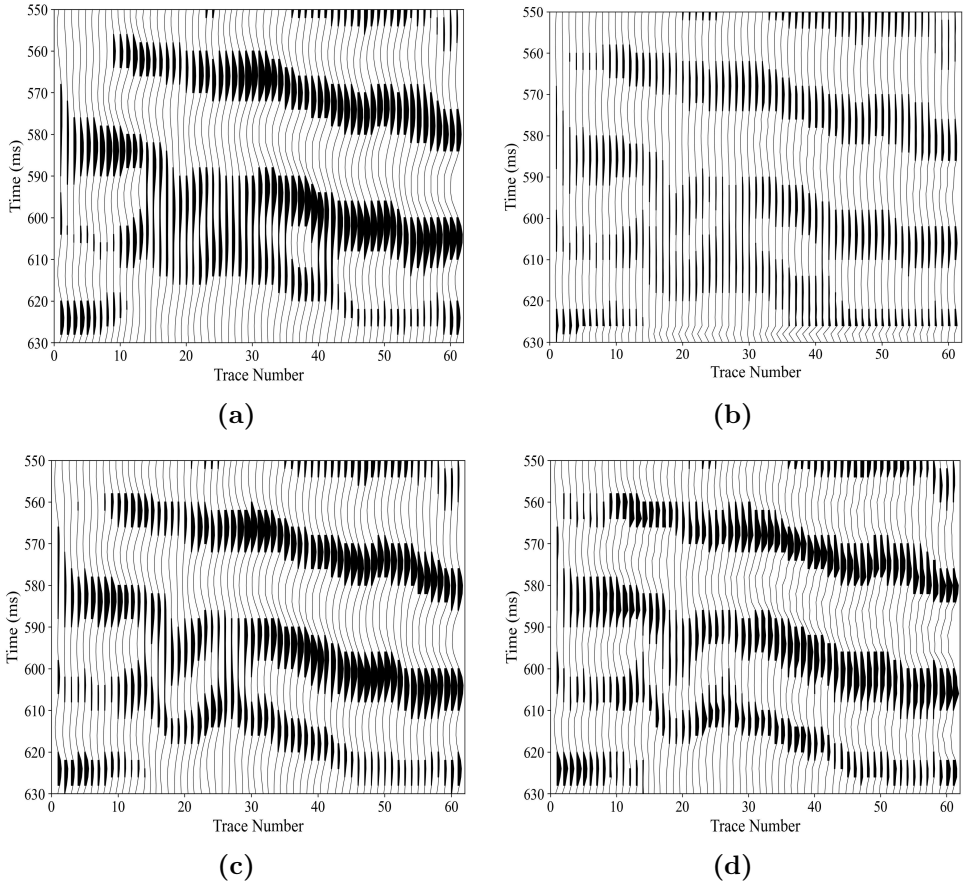


**Fig. 9** Magnified views of the low-resolution data and processing results. **a** Original low-resolution data; **b** IQF result; **c** U-Net result; **d** Result of the proposed method

significantly introduces high-frequency components, its results exhibit strong spatial instability; the seismic events show zigzag jitter, and background noise is excessively amplified, which compromises the lateral continuity of the geological sedimentation.

In contrast, the proposed method (Fig. 8**d**) significantly enhances vertical resolution while excellently maintaining the lateral continuity of seismic events. Particularly in the 3750–3850 ms interval, the proposed method successfully resolves the blurred composite waves from the original section into clear, layered structures with distinct reflection characteristics. At the strong reflection interface near 3450 ms, the proposed method provides sharper interlayer boundaries, making the detailed features of the geological structure more credible. These results validate the robustness of the network when processing field data.

To provide a more intuitive evaluation of the wavelet reconstruction capabilities of different methods, a local subset of traces (Traces 370–440) was selected for waveform comparison. As shown in Figs. 8**a** and 9**a**, the raw seismic data are constrained

by a low dominant frequency, and the wavelets exhibit severe side-lobe effects, leading to significant interference between adjacent reflection layers. Particularly in the 750–780 ms interval, where the interlayer travel time is less than the tuning thickness, multiple thin-bed reflections merge into a broad composite wave in the original record, masking the internal stratigraphic structures. Although Inverse Q-Filtering (IQF) compresses the wavelet to some extent and theoretically compensates for high-frequency components, experimental results (Figs. 8**b** and 9**b**) indicate that it suffers from low fidelity in the low-frequency band and fails to effectively eliminate the waveform interference caused by tuning effects, showing limited capability in recovering subtle geological details.

In contrast, deep learning-based methods demonstrate superior overall performance, where the overlapping broad peaks in the raw records are successfully resolved into distinct events with independent local extrema, consistent with the previous wedge model tests. However, as illustrated in Figs. 8**c** and 9**c**, the conventional U-Net is often limited by its architecture and fails to fully capture complex spectral mapping relationships, resulting in insufficient high-frequency enhancement.

The proposed method exhibits the most robust comprehensive performance. It not only achieves reliable feature recovery under low-frequency backgrounds but, more importantly, effectively decouples the interference-laden composite signals into high-resolution thin-bed responses. While significantly boosting the high-frequency content, the proposed method maintains excellent lateral continuity and natural morphological variations of the seismic events (Figs. 8**d** and 9**d**). The background remains clean, without the high-frequency artifacts or phase distortions typically induced by over-enhancement.

Spectral analysis further corroborates these findings (Fig. 10). In the raw data, the spectral energy is primarily concentrated between 10–40 Hz and attenuates rapidly beyond 40 Hz; this prominent spectral gap is the fundamental cause of the insufficient resolution. All three methods exhibit varying degrees of bandwidth extension. However, unlike the spectral energy shift toward the DC component in IQF or the limited bandwidth extension of the U-Net, the spectrum generated by the proposed method is smoother and maintains a consistent trend with the original low-frequency band. By significantly broadening the effective bandwidth while ensuring a reasonable energy concentration within the dominant frequency band, our method achieves optimal spectral enhancement. This indicates that the proposed network successfully infers and recovers the missing high-frequency harmonics from low-frequency data rather than simply amplifying noise.

To further verify the signal recovery characteristics of the network model across different frequency bands, and particularly to confirm the geological validity of the newly added high-frequency components, a spectral decomposition analysis was performed on the enhanced seismic data (Fig. 11). The data were decomposed into three intervals for display: low-frequency (0–20 Hz), mid-frequency (20–45 Hz), and high-frequency (45–80 Hz).

As shown in the figure, the low- and mid-frequency bands contain the primary energy and macroscopic structural information of the seismic data. The processed sections exhibit an extremely high signal-to-noise ratio (SNR) and clear stratigraphic

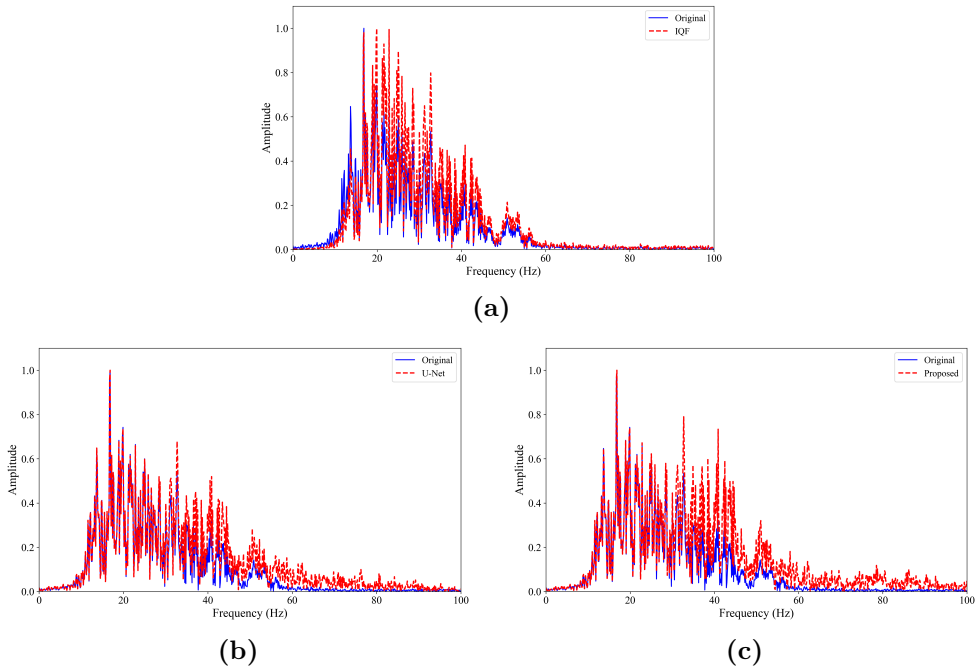


**Fig. 10** Comparison of amplitude spectra for the field data processing results. **a** IQF result spectrum; **b** U-Net result spectrum; **c** Spectrum of the proposed method, showing a smoother and broader bandwidth extension

sequences within these bands, indicating that the network perfectly preserves the large-scale background features and the primary structural framework of the original data during super-resolution processing, without introducing low-frequency distortions.

In the high-frequency interval (45–80 Hz), conventional methods often suffer from residual random noise or spatially discontinuous artifacts. In contrast, the high-frequency section processed by the proposed method displays clear and continuous seismic events, whose curvatures and morphologies are perfectly consistent with the structural attitudes observed in the low- and mid-frequency bands. These continuous high-frequency reflections are not disordered background noise but rather the successfully recovered genuine responses of thin-layers and minute sedimentary units. The network effectively injects structured energy into the high-frequency spectrum, thereby achieving a truly high-fidelity resolution enhancement.

# 5 Validation with Field Well Logs

To verify the geological reliability of the frequency-enhanced seismic data and quantitatively evaluate its resolution for thin layers, we conducted a well-tie calibration and comparative analysis using key exploration well J within the survey area, which possesses complete high-resolution sonic and density logs. Based on the seismic convolutional model theory, we first performed accurate time-depth conversion on the environmentally corrected log curves. Impedance curves were then calculated using

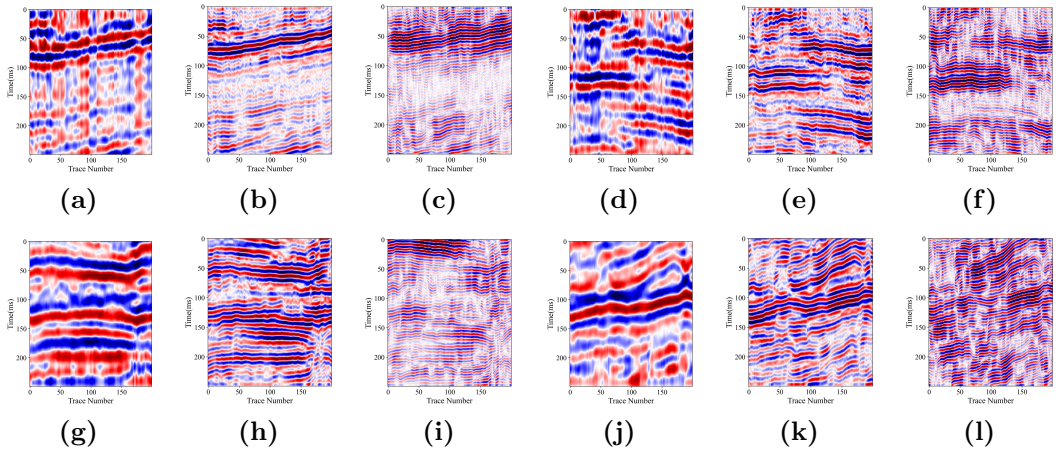


**Fig. 11** Comparison of multi-scale frequency-band decomposition. **a**, **d**, **g**, and **j** display the low-frequency components (0–20 Hz); **b**, **e**, **h**, and **k** show the mid-frequency components (20–45 Hz); **c**, **f**, **i**, and **l** present the high-frequency components (45–80 Hz)

the sonic velocity and density data, from which the reflection coefficient sequences representing true subsurface lithological variations were derived. Finally, high-resolution synthetic seismograms reflecting fine-scale geological structures were generated by convolving these sequences with a high-frequency wavelet.

Fig. 12 illustrates the integrated well-seismic analysis results passing through well J. From the reflection coefficient sequence (Fig. 12**d**), it can be observed that the target interval is characterized by dense alternating positive and negative pulses, indicating a typical thin-interbedded sedimentary environment in this region. The original seismic section (Fig. 12**a**) is constrained by a low dominant frequency and broad waveforms, resulting in significant interference effects where multiple thin-layer interfaces merge into a single strong reflection event, failing to accurately characterize the high-frequency details present in the reflection coefficient sequence.

In contrast, the frequency-enhanced seismic section (Fig. 12**e**) demonstrates a significant increase in vertical resolution while maintaining lateral continuity. A comparison between Fig. 12**d** and Fig. 12**e** reveals that the enhanced seismic events have become sharper, and more subtle reflection details have been resolved within the original high-amplitude zones. These details show excellent spatial correspondence with the stratigraphic variations in the reflection coefficient sequence, indicating that the processing results have faithfully recovered stratigraphic information previously masked by the side-lobes of the original wavelet.

To further quantitatively validate the accuracy of thin-layer identification, seismic traces adjacent to multiple wells were extracted for detailed waveform comparison, as shown in Fig. 13. In the figure, the red curves represent the ideal high-frequency synthetic records generated from well-log data, serving as the ground truth for thin-layer identification. Due to the low dominant frequency of the original seismic traces (black curves), they exhibit poor matching performance when compared to the 50 Hz high-frequency synthetic reference. In contrast, the seismic traces processed by the

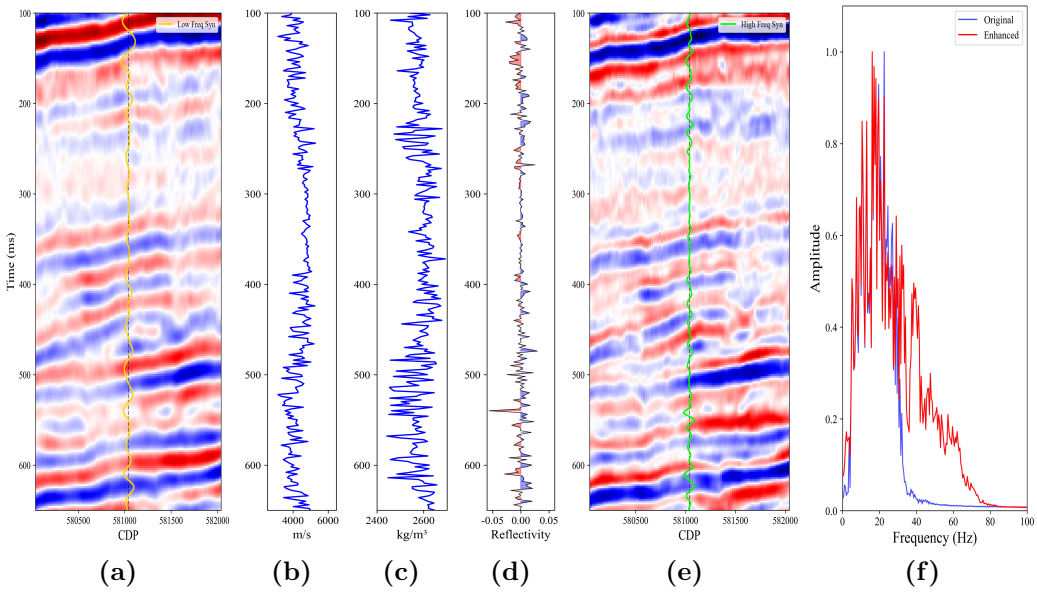


**Fig. 12** Well-seismic calibration of Well J. **a** Original seismic section; **b** Velocity log (m/s); **c** Density log (kg/m$^3$); **d** Reflection coefficients; **e** Enhanced seismic section; **f** Comparison of amplitude spectra before and after enhancement.

proposed method (green curves) successfully achieve wavelet compression and waveform decoupling, clearly resolving independent reflection events that were previously masked at several key stratigraphic levels.

Statistical results indicate that the cross-correlation coefficients between the original seismic data and the synthetic records range from 0.41 to 0.61. However, the correlation coefficients for the enhanced seismic data significantly improve to a range of 0.80 to 0.89. This high degree of fitting demonstrates that the frequency-enhanced seismic data closely approximate the true subsurface geological conditions in terms of both phase and amplitude characteristics. Taking the target interval from 1100 ms to 1200 ms as an example, the original trace appears as a broad composite wave, obscuring the internal sequence boundaries. Conversely, the enhanced trace exhibits clear waveform splitting and sharpening features, with its morphology highly overlapping the red synthetic record. These changes in waveform characteristics are not random noise but correspond to genuine reflections from the top and bottom interfaces of thin layers. This provides strong evidence that the proposed method effectively suppresses wavelet side-lobe effects, breaks through the limitations of traditional tuning thickness, and provides a high-fidelity data foundation for subsequent reservoir prediction.

# 6 Conclusion

This paper presented a novel deep learning framework, the Frequency-Domain Constrained Residual Fully Convolutional Network (FGC-Net), for high-fidelity seismic thin-layer resolution enhancement. The method addresses key limitations of traditional

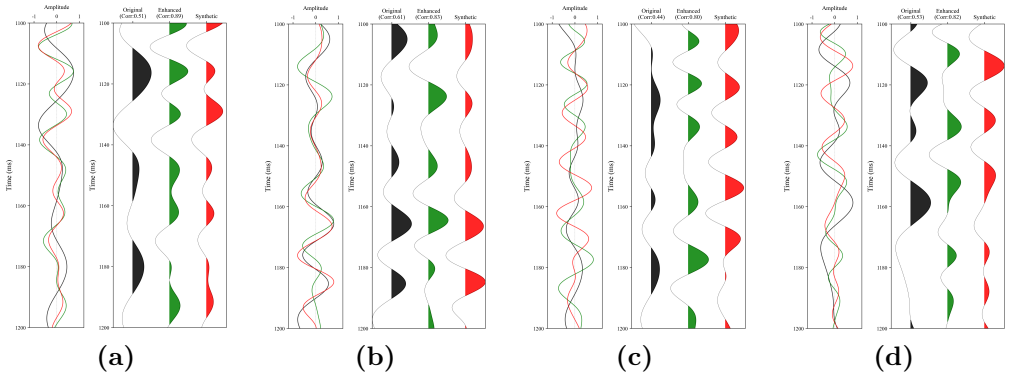


**Fig. 13** Waveform comparison between the seismic traces and synthetic seismograms. The black, green, and red lines represent the original seismic trace, the enhanced trace by the proposed method, and the high-frequency synthetic seismogram derived from well logs, respectively

approaches and conventional deep networks by integrating a physics-guided label generation strategy, a multi-scale encoder with Receptive Field Adaptive Modules, and explicit frequency-domain constraints via Frequency-Domain Residual Blocks. The joint loss function enforcing time-domain, spectral, and spatial consistency ensures the recovery is both high-resolution and geologically plausible.

Comprehensive tests on synthetic wedge models and field datasets demonstrated that the proposed method significantly extends the effective bandwidth, resolves thin layers at and beyond the theoretical tuning thickness, and maintains excellent lateral continuity and amplitude fidelity. Well-tie calibration confirmed the geological validity of the recovered high-frequency components, with correlation coefficients to synthetic records improving from 0.41–0.61 to 0.80–0.89. The framework provides a robust, data-driven solution for enhancing seismic resolution, particularly beneficial for the characterization of thin-bed reservoirs and complex geological structures.

## References

Alaei, N., Roshandel Kahoo, A., Kamkar Rouhani, A., & Bahroudi, M. (2018). Seismic resolution enhancement using scale transform in the time-frequency domain. *Geophysics*, 83(6), V305–V314. https://doi.org/10.1190/geo2017-0414.1

Cao, S., & Yang, D. (2016). A review of high-resolution seismic data processing approaches. *Xinjiang Petroleum Geology*, 37(1), 1–8.

Chen, H., Gao, J., Liu, N., & Zhang, J. (2019). Multitrace semiblind nonstationary deconvolution. *IEEE Geoscience and Remote Sensing Letters*, 16(8), 1195–1199. https://doi.org/10.1109/LGRS.2019.2892414

Chen, H., Sacchi, M.D., Haghshenas Lari, H., & Gao, J. (2023). Nonstationary seismic reflectivity inversion based on prior-engaged semisupervised deep learning method. *Geophysics*, 88(1), WA115–WA128. https://doi.org/10.1190/geo2022-0124.1

Chen, S., Cao, S., Sun, Y., & Gao, J. (2022). Seismic time-frequency analysis via time-varying filtering based empirical mode decomposition method. *Journal of Applied Geophysics*, 204, 104731. https://doi.org/10.1016/j.jappgeo.2022.104731

Chen, Z., Wang, Y., Chen, X., & Zhang, J. (2013). High-resolution seismic processing by Gabor deconvolution. *Journal of Geophysics and Engineering*, 10(6), 065002. https://doi.org/10.1088/1742-2132/10/6/065002

Das, V., Pollack, A., Wollner, U., & Mukerji, T. (2019). Convolutional neural network for seismic impedance inversion. *Geophysics*, 84(6), R869–R880. https://doi.org/10.1190/geo2018-0838.1

Deng, F., Wang, S., Wang, X., & Chen, Y. (2024). Seismic data reconstruction based on conditional constraint diffusion model. *IEEE Geoscience and Remote Sensing Letters*, 21, 1–5. https://doi.org/10.1109/LGRS.2024.3350123

Gao, Y., Zhao, D., Li, T., & Zhang, H. (2023). Deep learning vertical resolution enhancement considering features of seismic data. *IEEE Transactions on Geoscience and Remote Sensing*, 61, 1–13. https://doi.org/10.1109/TGRS.2023.3281055

Gao, Y., Zhang, J., Li, H., & Zhao, D. (2022). Incorporating structural constraint into the machine learning high-resolution seismic reconstruction. *IEEE Transactions on Geoscience and Remote Sensing*, 60, 1–12. https://doi.org/10.1109/TGRS.2021.3113994

Harsuko, R., & Alkhalifah, T. A. (2022). StorSeismic: A new paradigm in deep learning for seismic processing. *IEEE Transactions on Geoscience and Remote Sensing*, 60, 1–15. https://doi.org/10.1109/TGRS.2022.3174786

Ji, H. C., Wang, J., Liu, H. C., & Zhang, Y. (2022). Application of bidirectional extension frequency high-resolution seismic technique in Wuxia fault zone. *Progress in Geophysics*, 37(1), 201–212.

Li, J., Wu, X., & Hu, Z. (2021). Deep learning for simultaneous seismic image super-resolution and denoising. *IEEE Transactions on Geoscience and Remote Sensing*, 60, 1–11. https://doi.org/10.1109/TGRS.2021.3119918

Li, A., Chen, W., Wei, X., Zhang, H., Wang, H., & Chen, Y. (2025). Efficient unsupervised deep learning for simultaneous seismic noise attenuation and interpolation. *IEEE Transactions on Geoscience and Remote Sensing*, 63, 1–15. https://doi.org/10.1109/TGRS.2024.3412581

Lin, Y., Chen, S., Zhang, G., & Wang, H. (2022). High-resolution time-frequency analysis based on a synchroextracting adaptive S-transform and its application. *Journal of Geophysics and Engineering*, 19(5), 1124–1133. https://doi.org/10.1093/jge/gxac071

Liu, W., & Chen, W. (2026). Free-surface multiples attenuation based on seismic trace random arrangement via f-x variational mode decomposition. *Applied Geophysics*, 23(1), 1–9.

Liu, W., Yuan, G., & Chen, W. (2026). Random noise attenuation based on scale transformation stochastic resonance system and FXVMD. *Journal of Geophysics and Engineering*, 23, 1–9.

Liu, Q. W., Sun, Y. Z., & Li, Q. (2023). Application of frequency-division spectral blueing via synchrosqueezing wavelet transform in thin layer recognition. *Geophysical Prospecting for Petroleum*, 62(3), 529–537.

Liu, X., Wu, B., & Yang, H. (2023). Multitask full attention U-Net for prestack seismic inversion. *IEEE Geoscience and Remote Sensing Letters*, 20, 1–5. https://doi.org/10.1109/LGRS.2023.3284561

Manenti, R. R., Souza, W. E., & Porsani, M. J. (2018). Spectral whitening based on the singular spectral analysis method. *Journal of Geophysics and Engineering*, 15(4), 1460–1469. https://doi.org/10.1088/1742-2140/aaaf86

Margrave, G. F., Lamoureux, M. P., & Henley, D. C. (2011). Gabor deconvolution: Estimating reflectivity by nonstationary deconvolution of seismic data. *Geophysics*, 76(3), W15–W30. https://doi.org/10.1190/1.3560161

Oliveira, D. A. B., Ferreira, R. S., Silva, R., & de Souza, J. M. (2019). Improving seismic data resolution with deep generative networks. *IEEE Geoscience and Remote Sensing Letters*, 16(12), 1929–1933. https://doi.org/10.1109/LGRS.2019.2916581

Oliveira, S. A. M., & Lupinacci, W. M. (2013). L1 norm inversion method for deconvolution in attenuating media. *Geophysical Prospecting*, 61(4), 771–777. https://doi.org/10.1111/j.1365-2478.2012.01107.x

Paksima, S., Radad, M., Roshandel Kahoo, A., & Bahroudi, M. (2023). Identification of thin gas reservoir in reflection seismic data by synchrosqueezing S-transform in time-frequency representation. *Arabian Journal of Geosciences*, 16(6), 376. https://doi.org/10.1007/s12517-023-11484-0

Schuster, G. T., Chen, Y., & Feng, S. (2024). Review of physics-informed machine-learning inversion of geophysical data. *Geophysics*, 89(6), T337–T356. https://doi.org/10.1190/geo2023-0427.1

Sui, Y., & Ma, J. (2020). Blind sparse-spike deconvolution with thin layers and structure. *Geophysics*, 85(6), V481–V496. https://doi.org/10.1190/geo2019-0594.1

Sun, J., Innanen, K. A., & Huang, C. (2021). Physics-guided deep learning for seismic inversion with hybrid training and uncertainty analysis. *Geophysics*, 86(3), R303–R317. https://doi.org/10.1190/geo2020-0433.1

Sun, M., Li, Z., Li, Z., & Wang, Y. (2020). A noise attenuation method for weak seismic signals based on compressed sensing and CEEMD. *IEEE Access*, 8, 71951–71964. https://doi.org/10.1109/ACCESS.2020.2986278

Sun, Q. F., Xu, J.Y., Zhang, H.X., & Wang, Y. (2022). Random noise suppression and super-resolution reconstruction algorithm of seismic profile based on GAN. *Journal of Petroleum Exploration and Production Technology*, 12(8), 2107–2119. https://doi.org/10.1007/s13202-022-01466-9

Velis, D. R. (2008). Stochastic sparse-spike deconvolution. *Geophysics*, 73(1), R1–R9. https://doi.org/10.1190/1.2816669

Wang, B., Zhang, N., Lu, W., & Chen, Y. (2019). Deep-learning-based seismic data interpolation: A preliminary result. *Geophysics*, 84(1), V11–V20. https://doi.org/10.1190/geo2017-0635.1

Wang, L., Gao, J., Zhao, W., & Zhang, J. (2013). Enhancing resolution of nonstationary seismic data by molecular-Gabor transform. *Geophysics*, 78(1), V31–V41. https://doi.org/10.1190/geo2012-0050.1

Wang, N., Shi, Y., Ni, J., & Zhang, H. (2024). Enhanced seismic attenuation compensation: Integrating attention mechanisms with residual learning in neural networks. *IEEE Transactions on Geoscience and Remote Sensing*, 62, 1–11. https://doi.org/10.1109/TGRS.2024.3355102

Wang, S. Y., Chen, H., Hu, Y., & Liu, J. (2025). Multichannel seismic resolution enhancement via spectral fitting for thin reservoir characterization. *Petroleum Science*, 22(7), 2818–2827. https://doi.org/10.1016/j.petsci.2025.03.001

Wang, Y. (2002). A stable and efficient approach of inverse Q filtering. *Geophysics*, 67(2), 657–663. https://doi.org/10.1190/1.1468627

Wang, Y. (2006). Inverse Q-filter for seismic resolution enhancement. *Geophysics*, 71(3), V51–V60. https://doi.org/10.1190/1.2192939

Yang, L., Chen, W., Wang, H., & Zhang, Y. (2021). Deep learning seismic random noise attenuation via improved residual convolutional neural network. *IEEE Transactions on Geoscience and Remote Sensing*, 59(9), 7968–7981. https://doi.org/10.1109/TGRS.2020.3040316

Yang, L., Fomel, S., Wang, S., & Chen, W. (2023). Denoising of distributed acoustic sensing data using supervised deep learning. *Geophysics*, 88(1), WA91–WA104. https://doi.org/10.1190/geo2022-0192.1

Zhang, Y., Zhang, Y., Dong, H., & Gao, J. (2024). STUGAN: An integrated Swin transformer-based generative adversarial networks for seismic data reconstruction

and denoising. *IEEE Transactions on Geoscience and Remote Sensing*, 62, 1–15. https://doi.org/10.1109/TGRS.2024.3361102

# Statements and Declarations

## Funding

This work was supported in part by the Cooperative Innovation Center of Unconventional Oil and Gas (Grant No. UOG2024-19), the Open Research Fund of Key Laboratory of Engineering Geophysical Prospecting and Detection of Chinese Geophysical Society, the Meteorological Information and Signal Processing Key Laboratory of Sichuan Higher Education Institutes of Chengdu University of Information Technology, the Opening Fund of Geomathematics Key Laboratory of Sichuan Province, the Open Fund of Key Laboratory of Exploration Technologies for Oil and Gas Resources (Yangtze University), Ministry of Education (Grant No. K2024-18), and in part by the Foundation of National Key Laboratory of Uranium Resources Exploration-Mining and Nuclear Remote Sensing (Grant No. 2024QZ-TD-13).

## Competing Interests

The authors have no relevant financial or non-financial interests to disclose.

## Author Contributions

All authors contributed to the study conception and design. Material preparation, geological scenario modeling, and field data collection were performed by Jiaxin Yang and Wei Chen. The neural network architecture implementation, deep learning training, and spectrum analysis were carried out by Yaming Yang. Well-seismic calibration and synthetic seismogram generation were conducted by Jiaxin Yang. The first draft of the manuscript was written by Jiaxin Yang, and all authors commented on previous versions of the manuscript. All authors read and approved the final manuscript.